XMM–Newton and the Pleiades – I. Bright coronal sources and the X-ray emission from intermediate-type stars

K. R. Briggs[1,2]⋆ and J. P. Pye[1]⋆

[1]*X-ray Astronomy Group, Department of Physics and Astronomy, University of Leicester, Leicester LE1 7RH*
[2]*Paul Scherrer Institut, CH-5232 Villigen PSI, Switzerland*

ABSTRACT

We present results of X-ray spectral and timing analyses of solar-like (spectral types F5–K8) and intermediate-type (B4–F4) Pleiads observed in a 40-ks *XMM–Newton* EPIC exposure, probing X-ray luminosities (L_X) up to a factor 10 fainter than previous studies using the *ROSAT* PSPC. All eight solar-like members have 'quasi-steady' $L_X \gtrsim 10^{29}$ erg s^{-1}, consistent with the known rotation–activity relation and four exhibit flares. Using a hydrodynamic modelling technique, we derive loop half-lengths $\mathcal{L} \lesssim 0.5 R_\star$ for the two strongest flares, on H II 1032 and H II 1100. Near the beginning of its flare, the light curve of H II 1100 shows a feature with a profile suggestive of a total occultation of the flaring loop. Eclipse by a substellar companion in a close orbit is possible but would seem an extraordinarily fortuitous event; absorption by a fast-moving cloud of cool material requires N_H at least two orders of magnitude greater than any solar or stellar prominence. An occultation may have been mimicked by the coincidence of two flares, though the first, with its decay time being shorter than its rise time and suggestive of $\mathcal{L} \sim 0.02 R_\star$, would be unusual.

Spectral modelling of the quasi-steady emission shows a rising trend in coronal temperature from F and slowly rotating G stars to K stars to fast-rotating G stars, and a preference for low coronal metallicity. These features are consistent with those of nearby solar-like stars, although none of the three stars showing 'saturated' emission bears the significant component at 2 keV seen in the saturated coronae of AB Dor and 47 Cas. Of five intermediate-type stars, two are undetected ($L_X < 4 \times 10^{27}$ erg s^{-1}) and three show X-ray emission with a spectrum and L_X consistent with origin from an active solar-like companion.

Key words: stars: activity – stars: coronae – stars: early-type – stars: late-type – open clusters and associations: individual: Pleiades – X-rays: stars.

1 INTRODUCTION

The Pleiades is the archetypal stellar sample with age of ≈100 Myr and near-solar photospheric metallicity. Relative youth, proximity, compactness and richness make it key to understanding stellar X-ray emission and its evolution. Cluster members cover spectral types from late B to late M, enabling the simultaneous study of the different processes driving X-ray emission from stars of different internal structure.

Solar-like stars (spectral types ≈ F5–M3) have radiative cores and convective outer envelopes, and X-ray emission is believed to be from hot plasma confined in magnetic loops in the corona, a strong magnetic field being generated by a dynamo located at the base of the convection zone ($\alpha\Omega$ dynamo: Parker 1975), as on the

Sun. Supportive correlations of increasing coronal X-ray and chromospheric line (e.g. Hα, Ca II H, K) luminosities with increasing convection zone depth and increasing rotation rates have been well-observed (Pallavicini et al. 1981; Noyes, Weiss & Vaughan 1984; Pizzolato et al. 2003), although the saturation of these 'magnetic activity indicators' at high rotation rates, at an X-ray-to-bolometric luminosity ratio of $L_X/L_{bol} \approx 10^{-3}$ (Vilhu 1984), awaits a full explanation. X-ray luminosities, L_X, may exceed 10^3 times that of the Sun at the peak of its activity cycle and younger stellar samples show higher mean L_X as rotation rates slow with time through the braking effect of a magnetized stellar wind. The youth of the Pleiades ensures a number of 'ultrafast-rotating' solar-like members (UFRs), showing saturated levels of magnetic activity, of which there are few examples in the nearby field.

The X-ray-emitting corona of the Sun is highly variable and highly structured. Stellar X-ray emission is also highly variable, exhibiting flares with profiles echoing those seen on the Sun, though

⋆E-mail: briggs@astro.phys.ethz.ch (KRB); pye@star.le.ac.uk (JPP)

reaching a peak L_X of up to 10^3 times higher. X-ray telescopes cannot resolve stellar coronae into active regions and individual loops as seen on the Sun, but loop sizes may be inferred from analysis of flare decays (Reale & Micela 1998). Loop lengths that are a large fraction of, but smaller than, the stellar radius have been derived from flares observed on a small number of nearby solar-like stars (e.g. Maggio et al. 2000; Covino et al. 2001; Güdel et al. 2001). Younger, faster-rotating, samples show flares of higher peak L_X and with higher frequency (Stelzer, Neuhäuser & Hambaryan 2000), hence the Pleiades is a good target for the study of stellar flares and coronal structure.

The temperature structure and composition of some stellar coronae diverge from those of the solar corona. Therein, the bulk of X-ray-emitting plasma is at 1–2 MK (e.g. Orlando, Peres & Reale 2000), though flaring plasma is often as hot as 10 MK (Reale, Peres & Orlando 2001), while faster-rotating stars have more plasma at higher temperatures (e.g. Güdel, Guinan & Skinner 1997), with the most active stars having significant amounts of plasma at 20 MK (e.g. Mewe et al. 1996). Elemental abundances in the solar corona differ from those in its photosphere (so-called *solar abundances*), with elements with low first ionization potential (FIP), such as Fe, appearing *overabundant* (Meyer 1985), although variability occurs with location within the corona (McKenzie & Feldman 1992) and during flares (Reames, Meyer & von Rosenvinge 1994). In the coronae of highly active solar-like stars, however, low-FIP elements appear *underabundant* (e.g. Singh et al. 1999), and the FIP dependence of coronal abundances changes according to activity level (Audard & Güdel 2002). The proximity of the Pleiades enables the study of temperature structure and composition in coronae of a number of individual solar-like stars, helping to extend the relatively small sample of coronae in which these physical conditions have been measured.

While solar-like stars have hot coronae and early-type ($\lesssim$B3) stars are thought to generate X-rays via hot shocks within their massive stellar winds, stars of intermediate type ($\approx$B4–F4) lack both a deep convective envelope and a massive stellar wind and are thus generally considered incapable of strong X-ray emission: any observed is conventionally attributed to a later-type companion with a hot corona (e.g. Golub et al. 1983; Micela et al. 1996, 1999), although in most cases such a companion remains undiscovered. Intermediate-type Pleiads, relatively close and well studied for binarity, provide a good sample in which to test this assertion.

The X-ray emission from low-mass stars (spectral types $\gtrsim$M3), which are thought to be fully convective and hence unable to support an $\alpha\Omega$ dynamo, is examined in a companion paper (Briggs & Pye 2003).

The core of the Pleiades has been extensively surveyed at X-ray wavelengths by the *Einstein* (Caillault & Helfand 1985; Micela et al. 1990) and *ROSAT* (Stauffer et al. 1994; Micela et al. 1996, 1999; Stelzer & Neuhäuser 2001) observatories, and a single field therein has been observed twice by *Chandra* (Krishnamurthi et al. 2001; Daniel, Linsky & Gagné 2002, henceforth DLG02).

The *ROSAT* surveys detected X-ray emission, attributed to the coronae of late-type companions, from $\approx$ one-third of intermediate-type stars (Stauffer et al. 1994; Micela et al. 1996). Krishnamurthi et al. (2001) judged the soft, bright X-ray emission of four intermediate-type stars in the *Chandra* field to be intrinsic to these stars, but their known binarity led DLG02 to implicate solar-like secondaries.

The *ROSAT* surveys indicated X-rays were emitted by practically all solar-like Pleiads. Gagné, Caillault & Stauffer (1995, henceforth GCS95) analysed the individual spectra of X-ray-bright Pleiads

($\log L_X \gtrsim 30.0$) and the composite spectra of samples subdivided by spectral type (F, G, K, M) and into slow ($v \sin i < 16$ km s^{-1}) and fast ($v \sin i > 16$ km s^{-1}) rotators. Only among G stars did the rotation rate seem to cause significant spectral differences, but there was a rising sequence in temperature from F to slowly rotating G then K and M to fast-rotating G. GCS95 did not investigate coronal abundances due to the low energy resolution of the PSPC, but DLG02 found evidence for low Fe abundance in the coronae of three K stars.

Flares identified in the *ROSAT* surveys showed L_X increases of factors of 2–40, peak $\log L_X$ of 29.8–31.2 and decay time-scales of 1–13 ks, and were more frequent on K and M stars than on G stars, which have lower mean L_X/L_{bol} (GCS95; Stelzer et al. 2000). GCS95 inferred a loop half-length of $\mathcal{L} \gtrsim 6R_\star$ (stellar radii), for a large flare on the K star H ɪɪ 1516 using a quasi-static cooling loop model, but this model is not self-consistent in its assumptions and overestimates the loop length (Reale 2002), the energy range of the PSPC was insufficient to constrain the peak temperature and the light curve was sparsely sampled.

In comparison with *ROSAT*, the greater sensitivity, wider energy range, better energy resolution and continuous time coverage of the EPIC detectors onboard *XMM–Newton* enable spectral studies at higher resolution of Pleiades members with lower X-ray luminosities, the detection of smaller flares, and better-constrained modelling of large flares. We use the *XMM–Newton* EPIC cameras to perform spectral and timing analyses of stars of spectral types B–K in a single 15-arcmin radius field in the core of the Pleiades, with the aims: (i) to estimate the temperature structure and the metallicity and, through analysis of the decays of large flares, the loop size in the coronae of individual solar-like Pleiads and hence to compare these properties with those of well-studied coronae of nearby solar-like stars and (ii) to see whether X-ray emission from intermediate-type stars is consistent with emission from the coronae of later-type companions. DLG02 addressed similar questions using their 60-ks *Chandra* study of a neighbouring field. While the better angular resolution of *Chandra* offered lower background count-rates, our *XMM–Newton* observation adds to this study by sampling a more complete range of spectral types, providing more counts per source to enable better-constrained spectral modelling, expanding the sample of well-studied X-ray-detected intermediate-type Pleiads and being able to analyse large flares.

The paper is organized as follows. Section 2 describes the membership, optical and physical data on the Pleiades used in this work; Section 3 details the X-ray observations and data analysis performed; Section 4 reports and discusses our results; Section 5 summarizes the work.

2 PLEIADES MEMBERSHIP AND PHYSICAL PARAMETERS

We have drawn a list of solar-like and intermediate-type Pleiades members from the catalogue of Belikov et al. (1998), whose survey used optical (*BVR*) photometry, complete to $V \approx 17$, and proper-motion measurements, with a baseline of 23 or 30 yr, to determine membership. Henceforth we use the terms 'Pleiads' or 'members' to refer to stars included in this catalogue. The *XMM–Newton* EPIC field of view (FOV), its position within the Pleiades shown in Fig. 1(a), contains 13 such members, for which the individual positions in an optical image of the field are marked in Fig. 1(b). There are examples of each spectral type within the range of
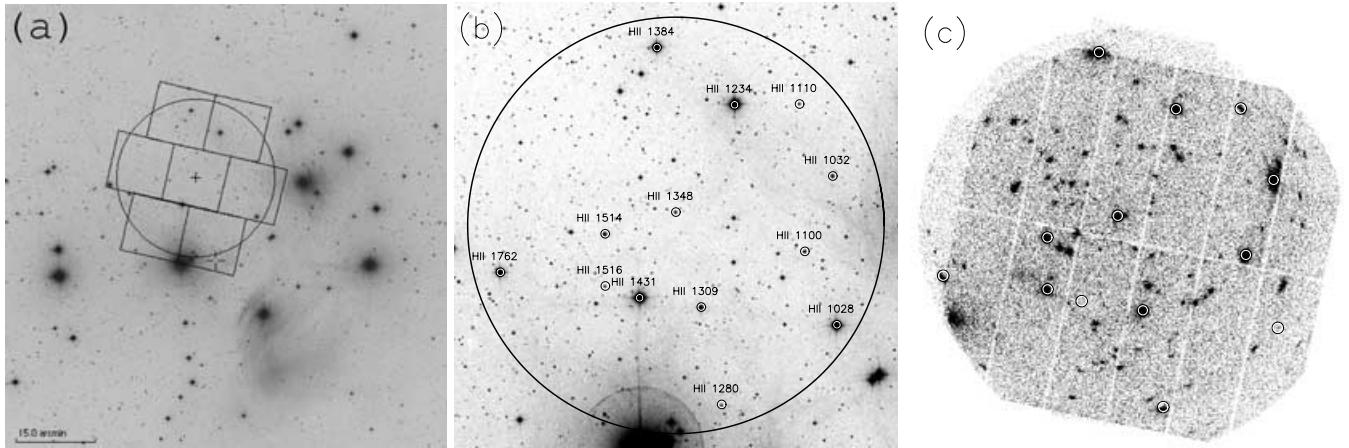
Figure 1. Images of the Pleiades *XMM–Newton* field. (a) Position of the EPIC FOV in the Pleiades [Digitized Sky Survey (DSS) image; overlaid MOS2 field from ALADIN]. (b) DSS optical image. The large circle marks the 30-arcmin diameter FOV of EPIC. (c) Mosaicked EPIC (MOS1+MOS2+pn) X-ray (0.3–4.5 keV) image. In (b) and (c), the positions of intermediate-type and solar-like Pleiads are circled.

Table 1. Data for Pleiades members in the EPIC field. Columns show: (2) spectral type (SIMBAD), (3) and (4) RA and Dec. (J2000) from USNO-A2.0 (Monet et al. 1998); (5) and (6) V (Belikov et al. 1998) and 2MASS J magnitudes (Cutri et al. 2000); (7) log L_{bol} in erg s^{-1}; (8) stellar radius in 10^{10} cm; (9) proper motion membership probability (Belikov et al. 1998); (10) and (11) projected rotational velocity in km s^{-1} and reference: 1. Soderblom et al. (1993); 2. Queloz et al. (1998); 3. Terndrup et al. (2000); (12) and (13) rotation period in d. Reference: 4. Marilli, Catalano & Frasca (1997); 5. Krishnamurthi et al. (1998); ':' indicates $P_{rot}/\sin i$ has been calculated from $v \sin i$ and $R_\star$; (14) flag noting spectroscopic (SB), visual (VB) and suspected photometric (Ph?) binaries (references in Section 4, Table 4).

H II (1)	SpT (2)	RA (3)	Dec. (4)	V (5)	J (6)	$[L_{bol}]$ (7)	$R_\star$ (8)	P_{mem} (9)	$v \sin i$ (10)	Ref. (11)	P_{rot} (12)	Ref. (13)	Bin. (14)
1234	B9.5V	3 46 59.40	+24 31 12.4	6.82	6.67	35.15	13.3	0.23	260	1	0.37	:	VB
1431	A0V	3 47 29.45	+24 17 18.0	6.81	6.61	35.15	13.3	0.61	40	1	2.4	:	SB
1028	A2V	3 46 27.10	+24 15 21.2	7.35	7.11	34.85	11.8	0.73	110	1	0.78	:	VB
1384	A4V	3 47 23.97	+24 35 20.0	7.66	7.12	34.70	11.3	0.83	215	1	0.38	:	Ph?
1762	A9V	3 48 13.50	+24 19 07.5	8.27	7.50	34.43	10.6	0.87	180	1	0.43	:	SB, VB
1309	F6V	3 47 09.98	+24 16 37.9	9.46	8.53	33.97	8.7	0.70	85	1	0.74	:	
1514	G5	3 47 40.38	+24 21 54.6	10.48	9.32	33.59	6.8	0.65	14	2	3.33	4	
1032	G8V	3 46 28.36	+24 26 04.2	11.34	9.62	33.28	5.8	0.95	37	2	1.31	5	Ph?
1100	K3V	3 46 37.22	+24 20 38.8	12.16	10.12	33.03	5.1	0.35	5	2	7.4	:	VB
1348	K5	3 47 17.99	+24 23 28.9	12.61	10.38	32.89	4.8	0.01	5	2	6.9	:	SB
1110	K6.5e	3 46 38.83	+24 31 15.1	13.29	11.04	32.69	4.2	0.98	6	2	5.1	:	
1516	K	3 47 40.30	+24 18 09.3	14.02	11.14	32.47	3.7	0.75	105	2	0.25	:	Ph?
1280	K8	3 47 03.52	+24 09 37.0	14.55	11.63	32.31	3.3	0.64	85	3	0.30	5	

interest: one B, four A, one F, two G and five K stars. These members are identified throughout the paper using H II numbers (table 2 of Hertzsprung 1947). Positional, photometric, rotational, binarity and membership data (where available) have been culled from the literature and are listed in Table 1. The sample includes one G-type and two K-type UFRs. We have further used a colour–magnitude diagram (Fig. 2) to highlight suspected photometric binaries. We adopt a distance to the Pleiades of 127 pc, $(m - M)_0$ = 5.52 (e.g. Stello & Nissen 2001) as used in previous X-ray surveys. Extinction, $A_V = 0.12$, and reddening, $E(B - V) = 0.04$, to the cluster are fairly uniform across the EPIC field (Stauffer 1984), and imply a hydrogen column density of $N_H = 2 \times 10^{20}$ cm^{-2} using the relation of Paresce (1984). The metallicity of the cluster is near-solar (e.g. King et al. 2000). We have inferred bolometric luminosities and stellar radii (the latter estimated through the Stefan–Boltzmann law) by interpolation, using M_V, of the Girardi et al. (2000) models for stars with solar metallicity and an age of 100 Myr.

3 X-RAY OBSERVATIONS AND DATA ANALYSIS

Observation 0094780101 was a guaranteed time pointing (PI: M. Watson) centred on the brown dwarf Teide 1 (J2000: $\alpha =$ 03^h 47^m 18^s.0, $\delta = +24°$ 22′ 31″), performed on 2000 September 1, in orbit 134. An exposure time of 50 ks was scheduled but only 40.6 ks was achieved in the EPIC pn (Strüder et al. 2001) and 33.0 ks in each of the two EPIC MOS (Turner et al. 2001) detectors. The Thick filter was used in each of the three telescopes.

The data were processed using the SCIENCE ANALYSIS SYSTEM (SAS) version 5.2.[1] We filtered each eventlist to exclude 'bad' events (using the #XMMEA_EM and #XMMEA_EP filters for MOS and pn, respectively), uncalibrated event patterns (PATTERN >12 for MOS; PATTERN > 4 for pn), and visually identified 'hot' pixels. Several
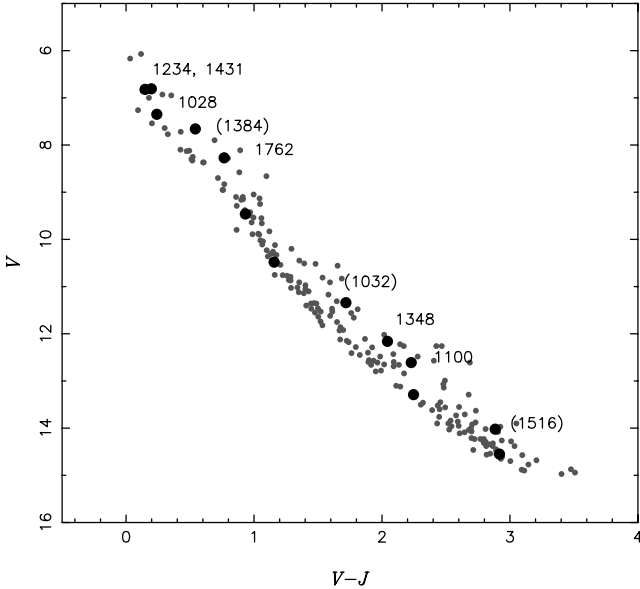
[1] http://xmm.vilspa.esa.es/

Figure 2. Colour–magnitude diagram for Pleiades members – in (black) and outside (grey) the EPIC FOV – indicating confirmed (bracketless) and suspected photometric (bracketed) binaries.

short background flares occurred but had no significant effect on the analysis of bright sources so affected periods were only excluded in the estimation of upper limits for undetected sources.

Fig. 1(c) shows a mosaic of images from all three EPIC cameras in the energy range 0.3–4.5 keV. All eight solar-like stars (F–K) and three of the five intermediate-type stars (B–A) were clear by-eye detections. We henceforth refer to these 11 stars collectively as 'X-ray-bright Pleiads'. The SAS source-detection software was run on images from the individual cameras, finding the best-fitting X-ray position to be within 3.5 arcsec of the optical position (USNO-A2.0: Monet et al. 1998) for each X-ray-bright Pleiad, and finding the remaining two intermediate-type Pleiads, H II 1028 and 1431, to be undetected at a maximum-likelihood threshold of $ML > 12$. Upper limits (at the 95 per cent confidence level) to their X-ray luminosities were estimated from the counts in the 0.3–4.5 keV band within 16 arcsec of the optical position (using the 'classical' prescription of Kraft, Burrows & Nousek 1991 and the algebraic approximations to the Poissonian upper limit derived by Gehrels 1986) by correcting for enclosed energy and effective exposure time, and assuming a 0.8-keV MEKAL source spectrum and a distance of 127 pc.

We performed spectral and timing analyses of the X-ray-bright Pleiads using primarily data from the pn, as its higher sensitivity and longer exposure time collected typically a factor of 3–4 more counts per source than a single MOS. MOS data were used where they provided $\gtrsim 500$ source counts and were not affected by CCD edges (H II 1384, 1762). For each X-ray-bright Pleiad, we extracted a spectrum and light curve from a circular region centred on the best-fitting X-ray source position. The radius of this circle, r, ranged from 30 to 60 arcsec and was constrained by two concerns: (i) contamination by neighbouring sources and (ii) retention of a good signal-to-noise ratio. The former provided the stronger constraint in most cases. In each case, a background spectrum and light curve were also extracted from a surrounding annulus, with inner radius $\geqslant 1.5r$ and area $\gtrsim 5$ times the source extraction area after areas contaminated by other sources had been removed. The number of background counts, B, expected to fall within each source extraction region was

estimated from background maps produced by the source detection procedure and each background product was scaled to contribute B counts to its associated source product. Analysis of the source products is described below.

3.1 Time series analysis

Source and background light curves were extracted (from regions described above) in the 0.3–4.5 keV band and binned to ensure an average of >20 net source counts per bin, to enable good approximation of the error on the total counts in each bin, N, as $\sqrt{N}$. Background-subtracted source light curves are displayed in Fig. 3.

We visually identified flare-like behaviour, defined as an isolated event of heightened emission peaking at a factor of >2 above the mean 'quasi-steady' level outside that event. The decay time-scale of each flare was estimated by fitting an exponential decay to the light curve, fixing the time of peak emission to the bin containing the peak number of counts. The peak and quasi-steady count-rates and the e-folding decay time-scale were fitted as free parameters. General variability was assessed by applying a χ^2 test against constancy to the background-subtracted source light curve. While the χ^2 test is flawed in that its result depends on the binning of data, we feel it is more robust than the Kolmogorov–Smirnov (K–S) test, which is applied to unbinned timing data but is not strictly applicable in the presence of a significant varying background, which is the case here. Flare parameters and results of the χ^2 test are given in Table 2.

3.2 Spectral analysis

In the extraction of spectra of variable sources, periods affected by clear flares (e.g. H II 1516) or non-flare-like high emission (e.g. H II 1234) were excluded to enable analysis of 'quasi-steady' emission, i.e. not strongly biased by a single transient event. Where sufficient counts were available, spectra from these periods were analysed separately. For each spectrum, an ancillary response file (ARF) was generated to account for bad pixels and chip gaps, the spatial variations of effective area and quantum efficiency, vignetting and losses due to the finite source extraction area. Finally, each source spectrum was grouped to a minimum of 20 counts per bin. All data bins containing fewer than 20 counts, and all data outside the range 0.3–4.5 keV, were ignored in spectral analysis. The latest (as of 2002 October) pn and MOS redistribution matrices were used, with the ARFs, to model the instrumental responses.

The X-ray emission of a stellar corona is due to hot, optically thin plasma and the spectrum is expected to be a superposition of the spectra of many individual loops of hot plasma at different temperatures. Hence, the form of the differential emission measure (DEM) as a function of temperature may be rather complex. Additionally, elemental abundances in coronae may differ from solar abundances. However, the relatively low energy resolution (≈ 70 eV) provided by EPIC, and signal-to-noise ratio typical of bright coronae at the distance of the Pleiades, require us to approximate the DEM to one (1-T) or two (2-T) discrete temperature components, and estimate abundances using a metallicity parameter, Z, in which the abundances of individual metals are fixed to the ratios observed in the solar photosphere but the total abundance of metals relative to that of H may be fixed to the solar value ($Z_\odot$) or fitted freely (Z_{free}). The MEKAL plasma emission code was used, and the absorbing column density was fixed to the nominal value for the Pleiades (see Section 2) of $N_H = 2 \times 10^{20}$ cm^{-2}, as exclusion of data below 0.3 keV prevents constraint of N_H at such low values.
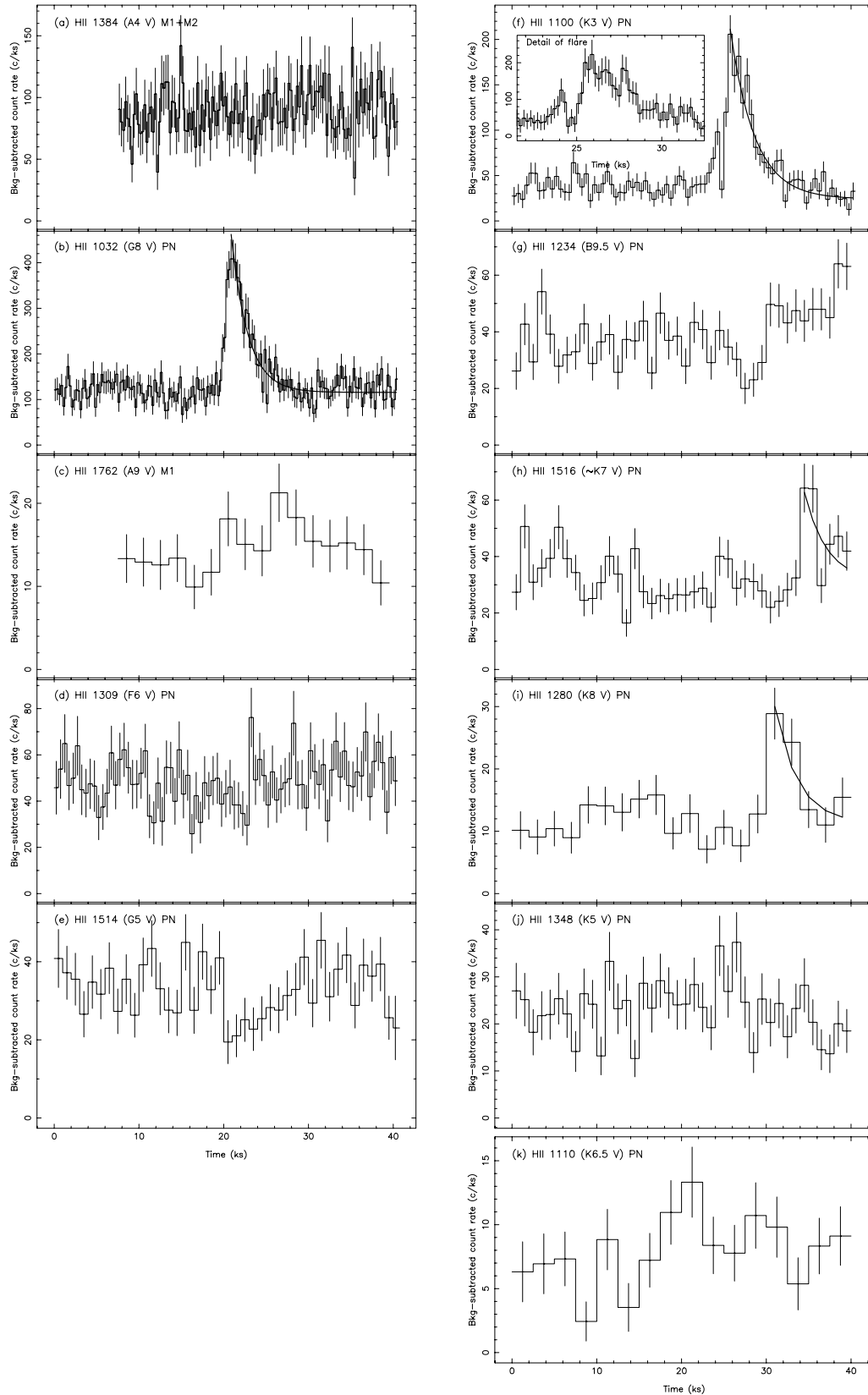
Figure 3. Light curves of X-ray-bright Pleiads in the *XMM–Newton* EPIC field. Each light curve is background-subtracted but not corrected for vignetting or enclosed energy, covers the same time range and is labelled with the source name, its spectral type, and the instrument(s) used. For the flaring sources (b, f, h, i) the best-fitting exponential decay is shown. The columns separate the *sources* by spectral type (as catalogued for the solar-like; as proposed in Section 4.3 for the intermediate-type Pleiads): F and G on the left; K on the right. The sources are ordered by quasi-steady L_X, decreasing from top to bottom.

Table 2. Results of time-series analysis of X-ray-bright Pleiads in the *XMM–Newton* EPIC field. Columns show: (2) instrument(s) used; (3) radius of extraction region for time-series and spectrum; (4) bin-size in time-series in s; (5) χ^2 probability of consistency with constant source emission. For flare-like variability: (6) peak $\log L_X$ in the 0.3–4.5 keV band in erg s^{-1}; (7) exponential decay time-scale (and 90 per cent confidence interval) in ks.

H II (1)	Ins (2)	r (3)	Δt (4)	$P(\chi^2)$ (5)	$[L_X]_{pk}$ (6)	τ_{LC} (90 per cent) (7)
1234	pn	50	1000	0.00		
1384	pn	60	500	0.04		
	M1	60	500	0.41		
	M2	60	500	0.14		
	M1+2	60	250	0.37		
1762	M1	50	2000	0.57		
1309	pn	50	500	0.63		
1514	pn	40	1000	0.17		
1032	pn	60	250	0.00	30.8	2.0 (1.7–2.3)
1100	pn	50	500	0.00	30.3	2.9 (2.6–3.3)
1348	pn	30	1000	0.07		
1110	pn	60	2500	0.04		
1516	pn	30	1000	0.00	29.7	2.6 (1.2–6.8)
1280	pn	40	2000	0.00	29.6	2.7 (1.5–4.7)

A model was considered to provide an acceptable fit to the data if a χ^2 test gave a null hypothesis probability of $\geqslant 0.10$. The addition or freeing of extra parameters (i.e. a temperature component or elemental abundance) was considered to produce a significantly improved fit if an F-test indicated the probability of an equal or larger improvement in χ^2 occurring by chance was $\leqslant 0.05$. The best-fitting models are displayed in Fig. 4, with parameters, and 90 per cent confidence intervals, listed in Table 3.

4 RESULTS AND DISCUSSION

4.1 Quasi-steady emission from solar-like stars

4.1.1 K-type stars

The five K stars exhibited quasi-steady L_X and L_X/L_{bol} values consistent with those expected (using empirical relations found by Pizolato et al. 2003) from their rotation periods and spectral types: in particular, those of the binary H II 1100 were consistent with twin K3 components (Bouvier, Rigaut & Nadeau 1997), each rotating with period $\sim$7 d, and the UFRs H II 1516 and 1280 showed saturated-level emission, although it should be noted that H II 1348 (Queloz et al. 1998) and possibly 1516 (Fig. 2) are also binary, with uncharacterized companions.

The quasi-steady spectra of the five K stars were remarkably similar: clearly flatter than those of the earlier-type stars H II 1514 and 1309 (see Fig. 4); requiring 2-T and/or Z_{free} models for acceptable fits, with $kT_1 \approx 0.35$ and $kT_2 \approx 1.0$ keV (Table 3), in fair agreement with the temperatures of 0.28 and 1.10 keV that best-fitted a composite *ROSAT* PSPC spectrum of a sample of Pleiades K stars (GCS95). The two spectral components have approximately equal emission measures, and although that of the hotter component is the lower for the two slowly rotating stars, H II 1348 and 1110, it is not significantly so. Fits to the better-quality spectra (>900 net source counts; H II 1100, 1348 and 1516 – cf. <500 counts for H II 1110 and 1280) were significantly improved by allowing non-solar metallicity in the 2-T model, with $Z \sim 0.2 Z_\odot$. DLG02 also found

evidence for low Fe abundances in the spectra of two K stars in the *Chandra* sample, and subsolar coronal metal abundances appear to be a consistent feature of nearby active K stars (AB Dor: Mewe et al. 1996; 'Speedy' Mic: Singh et al. 1999; LQ Hya: Covino et al. 2001).

4.1.2 H II 1032 (G8 V)

H II 1032 exhibited saturated-level X-ray emission, $\log L_X \approx 30.1$ and $\log(L_X/L_{bol}) \approx -3.1$, consistent with its rotation period of 1.33 d. The quasi-steady spectrum required a 2-T Z_{free} model with $kT_1 \approx 0.6$ and $kT_2 \approx 1.3$ keV with a ratio of hotter:cooler emission measures of $EM_2/EM_1 \sim 1.5$ and metallicity $Z \sim 0.3 Z_\odot$. A *ROSAT* PSPC spectrum of H II 1032 was best-fitted using temperatures of 0.4 and 1.2 keV, with fixed solar metallicity (GCS95). Comparable best-fitting temperatures were found for a composite PSPC spectrum of fast-rotating G-type Pleiads, and an individual spectrum of the fast-rotating G star H II 320 (GCS95; Fig. 5). In mass and saturated-level X-ray emission, H II 1032 resembles the nearby, faster-rotating ($P_{rot} = 0.514$ d) K0–1 star AB Dor, but while the quasi-steady spectrum of AB Dor also shows a component at 0.6 keV, it has a prominent hot component at 1.9 keV absent on H II 1032 (Mewe et al. 1996; Maggio et al. 2000; Güdel et al. 2001). The sample of well-studied solar-like UFRs is too small for the effect of saturation on coronal properties such as temperature, to be well-investigated so additions to this sample are important to our understanding of activity saturation. While no companion to H II 1032 has been reported (e.g. Bouvier et al. 1997), Fig. 2 suggests photometric binarity, so its X-ray emission may arise from the unsaturated coronae of two or more active stars.

4.1.3 H II 1514 (G5 V)

H II 1514 showed $\log L_X \approx 29.3$, consistent with its rotation period of 3.33 d. Its spectrum was acceptably fitted with a 1-T Z_{free} model with $kT \approx 0.55$ keV and $Z \sim 0.3 Z_\odot$. A second temperature was not constrained, but a significant component at $kT < 0.2$ keV could not be discounted. Hotter temperatures best-fitted both a composite *ROSAT* PSPC spectrum of slowly rotating G stars ($kT_1 \approx 0.23$, $kT_2 \approx 0.92$ keV), and individual spectra of two reportedly slow-rotating G stars, H II 739 and 761 (GCS95), though the L_X of these stars (>10^{30} erg s^{-1}) indicates *fast rotation* akin to the nearby solar-analogue EK Dra (Güdel et al. 1997). The slower-rotating ($P_{rot} \approx 5$ d), nearby G1 stars π^1 UMa and χ^1 Ori do show similar L_X and temperatures to H II 1514.

4.1.4 H II 1309 (F6 V)

H II 1309 gave $\log L_X \approx 29.4$ and a relatively soft X-ray spectrum, akin to that of H II 1514, acceptably fitted with a 1-T, $Z_\odot$ model with $kT \approx 0.56$ keV, although low metallicity, $Z \sim 0.5 Z_\odot$ offered significant improvement. As for H II 1514, a significant cool ($kT < 0.2$ keV) component could not be ruled out. Similar temperatures ($kT_1 < 0.2, 0.4 < kT_2 < 0.7$: mean 0.54 keV) and $\log L_X$ (28.5–29.5: mean 29.2) were found for a sample of field F stars (Panzera et al. 1999), although a composite spectrum of F-type Pleiads required a hotter temperature of $kT_2 \approx 0.69$ keV (GCS95). The rotation period of H II 1309 of $\lesssim 0.74$ d may suggest saturated-level activity. In late-F stars, saturation appears to set in at lower L_X/L_{bol} ($\sim 10^{-4}$) and perhaps shorter rotation periods than in G stars (Pizzolato et al. 2003).
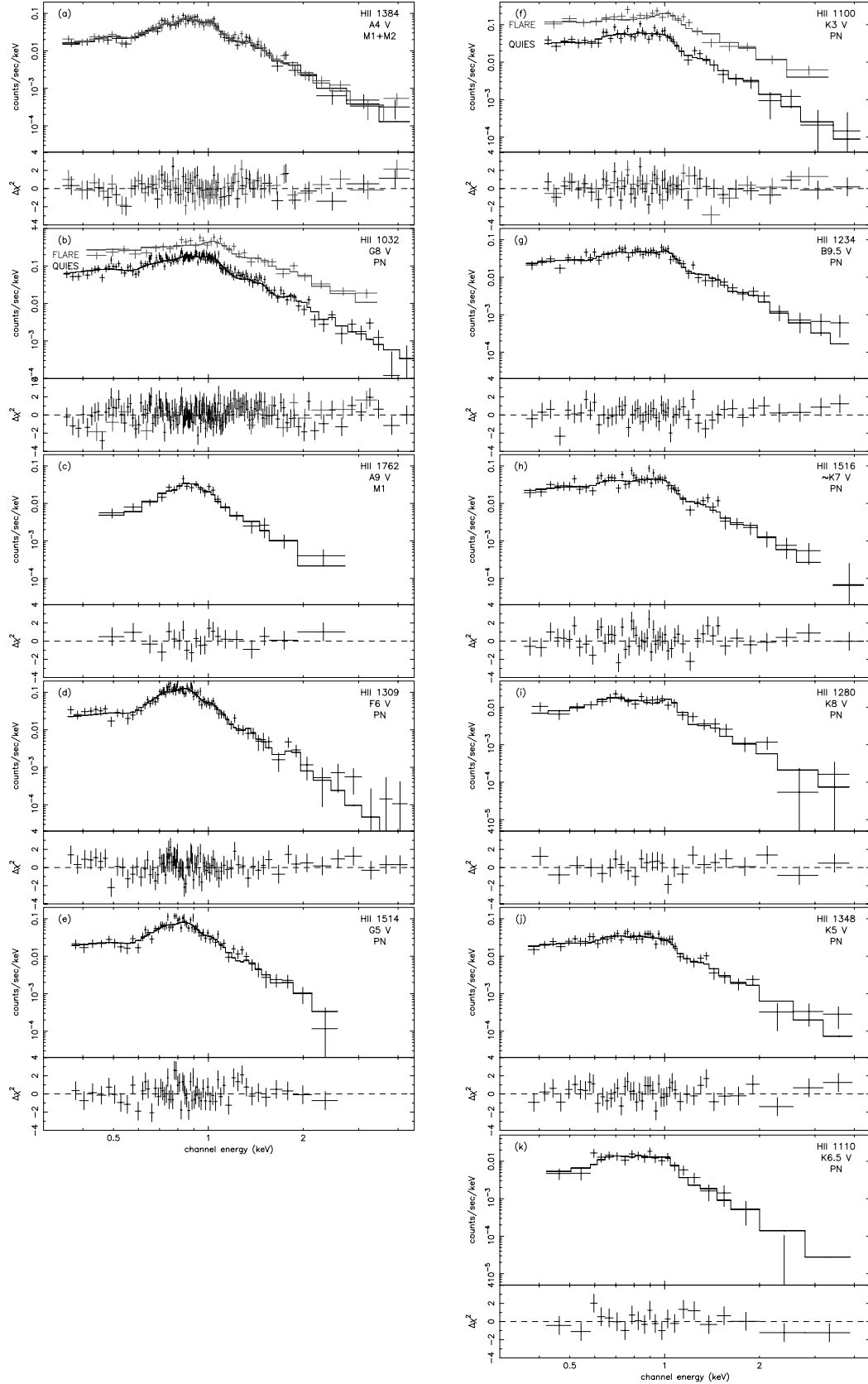
Figure 4. Quasi-steady spectra of X-ray-bright Pleiads in the *XMM–Newton* EPIC field. Each spectrum is labelled with the source name, its spectral type and the instrument(s) used. In (a), black and grey mark MOS1 and MOS2 data, respectively; in (b) and (f) grey marks the flare peak spectrum. The displayed model is as detailed in Table 3. The lower panel of each spectrum shows the χ^2 residuals. Spectra on the left (a–e) are, or resemble, those of F or G stars; spectra on the right (f–k) are, or resemble, those of K stars. Spectra are ordered by L_X, decreasing from top to bottom.

Table 3. Spectral parametrization of quasi-steady emission from X-ray-bright Pleiads in the *XMM–Newton* EPIC field. The fitting procedure is described in Section 3.2. Columns show: (2) instrument(s) used in fit; (3) net source counts in spectrum; (4) and (5) temperatures in keV of cooler and hotter components, respectively; (6) log emission measure of cooler component in cm^{-3}; (7) ratio of emission measures of hotter to cooler component; (8) metallicity; (9) log L_X in erg s^{-1} in 0.3–4.5 keV band; (10) log(L_X/L_{bol}); (11) χ^2/degrees of freedom and null-hypothesis probability. Columns (4), (5), (7) and (8) give the best-fitting value and (90 per cent confidence interval). The point spread function of H II 1384 is only partially included on the pn CCD, so no values are given for columns (6), (9) and (10).

H II (1)	Ins (2)	N_X (3)	kT_1 (90 per cent) (4)	kT_2 (90 per cent) (5)	$[EM_1]$ (6)	EM ratio (90 per cent) (7)	Z (90 per cent) (8)	$[L_X]$ (9)	$[L_X/L_{bol}]$ (10)	χ^2/ν (P) (11)
1234	pn	1051	0.37 (0.31–0.50)	1.08 (0.98–1.31)	52.18	1.49 (1.08–2.06)	0.26 (0.17–0.41)	29.53	−5.62	39/49 (0.86)
1384	pn	1908	0.50 (0.37–0.60)	1.02 (0.91–1.18)	–	0.84 (0.41–1.27)	0.26 (0.20–0.36)	–	–	79/79 (0.49)
	M1	1443	0.54 (0.45–0.63)	1.01 (0.88–1.27)	52.93	0.80 (0.30–1.22)	0.26 (0.19–0.37)	30.17	−4.53	42/50 (0.77)
	M2	1493	0.61 (0.49–0.66)	1.26 (0.94–1.94)	53.15	0.43 (0.18–1.02)	0.18 (0.13–0.26)	30.21	−4.49	42/53 (0.87)
	M1,2	2936	0.53 (0.49–0.58)	1.01 (0.95–1.35)	52.99	0.88 (0.42–1.06)	0.22 (0.17–0.27)	30.20	−4.50	90/107 (0.88)
1762	M1	485	0.64 (0.61–0.68)		52.19		1.00	29.63	−4.80	14/20 (0.82)
1309	pn	1982	0.56 (0.54–0.59)		52.26		0.54 (0.38–0.79)	29.48	−4.49	77/86 (0.74)
1514	pn	1347	0.56 (0.53–0.59)		52.29		0.29 (0.23–0.47)	29.31	−4.28	71/60 (0.15)
1032	pn	3674	0.62 (0.58–0.67)	1.23 (1.08–1.35)	52.72	1.48 (1.10–1.93)	0.33 (0.26–0.42)	30.14	−3.14	149/145 (0.40)
1100	pn	906	0.37 (0.30–0.47)	0.93 (0.83–1.09)	52.35	1.11 (0.80–1.80)	0.20 (0.13–0.50)	29.55	−3.48	37/41 (0.64)
1348	pn	942	0.34 (0.27–0.45)	0.94 (0.77–1.09)	52.03	0.78 (0.52–1.38)	0.18 (0.10–0.32)	29.12	−3.77	35/43 (0.79)
1110	pn	322	0.34 (0.28–0.42)	1.02 (0.79–1.29)	51.36	0.94 (0.58–1.47)	1.00	29.00	−3.69	17/18 (0.53)
1516	pn	1036	0.32 (0.25–0.40)	0.92 (0.78–1.04)	52.14	1.19 (0.87–2.44)	0.22 (0.13–0.36)	29.36	−3.11	56/48 (0.20)
1280	pn	432	0.32 (0.27–0.37)	1.32 (1.06–1.74)	51.56	1.39 (0.96–1.98)	1.00	29.22	−3.09	17/22 (0.76)

4.1.5 Overview

A rising sequence in coronal temperature (kT_1, kT_2 in keV) was observed from the F and slow-rotating G stars (<0.2, 0.55), through the K stars (0.3, 1.0) to the fast-rotating G star (0.6, 1.3), confirming an analysis of composite *ROSAT* PSPC spectra of Pleiads (GCS95), which showed the same trend, albeit with slightly different values, and largely in agreement with spectral analyses of field F stars,
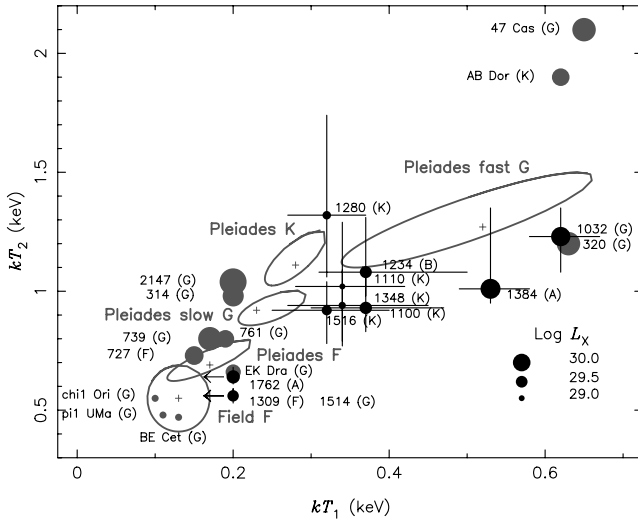

Figure 5. A comparison of coronal temperatures, using 2-T models, of Pleiads and nearby solar-like field stars. Filled black circles mark Pleiads in the EPIC FOV (Table 3); filled grey circles mark other individual Pleiads and field stars: the circle size represents the source L_X, and the H II number or source name, and (spectral type) are given. Open ellipses show (i) approximate 90 per cent confidence regions for Pleiads samples divided by spectral type and rotation rate; (ii) approximate limits for a sample of field F stars. Note the sequence in increasing temperature from F and slowly rotating G through K to fast-rotating G stars. The sources associated with the intermediate-type Pleiads 1762, 1384 and 1234 have L_X, kT_1, kT_2 consistent with those of solar-like stars.

using *ROSAT* (Panzera et al. 1999), and nearby solar analogues, using *ROSAT* and *ASCA* (Güdel et al. 1997, 1998), although none of our Pleiades sample has a significant component as hot as 2 keV as do 47 Cas and AB Dor (see Fig. 5).

We also found a requirement or significant preference for subphotospheric metallicities in the quasi-steady spectra of all solar-like Pleiads providing >500 source counts: $Z \sim 0.2$ Z$_\odot$ for K stars, $\sim$0.3 Z$_\odot$ for G stars and $\sim$0.5 Z$_\odot$ for the F star. The fitted metallicity, Z, is typically driven by the abundance of Fe, which has strong emission lines in the EPIC energy range. High-resolution X-ray spectroscopy of nearby solar-like stars has found coronal elemental abundances to depend on FIP in a manner that changes with L_X/L_{bol} or coronal temperature (Audard & Güdel 2002). In highly active stars, such as AB Dor, low-FIP elements such as Fe appear underabundant, while in intermediate-activity stars, such as π^1 UMa or χ^1 Ori, there is no FIP bias, and in low-activity stars, such as the Sun, low-FIP elements appear overabundant (Meyer 1985). The low values of Z we find in the coronae of the active G- and K-type Pleiads H II 1032, 1100 and 1516 appear to fit into this framework, but the similarly low Z of the intermediate-activity H II 1514 does not. Coronal abundances are entangled with the emission measure distribution in spectra of this quality, and are much better studied with instruments that can resolve individual lines and measure *relative* abundances of different elements, not just a global metallicity parameter. Overall our results indicate that the temperature structure and abundances in the quasi-steady coronae of solar-like Pleiads conform to expectations from well-studied nearby active stars.

4.2 Variability and flaring on solar-like stars

All five K stars exhibited variability at the 90 per cent confidence level – only in H II 1348 was the light curve consistent with constant emission with probability >0.05 – and H II 1100, 1516 and 1280 displayed flare-like events (Figs 3f, h and i). All three flares had decay time-scales, τ_{LC}, of $\sim$3 ks. The H II 1100 flare outshone the rest of its corona five times over, while the peak L_X of the flares on H II 1516 and 1280 just exceeded those of their respective quasi-steady coronae. The light curve of H II 1100 shows a striking dip near
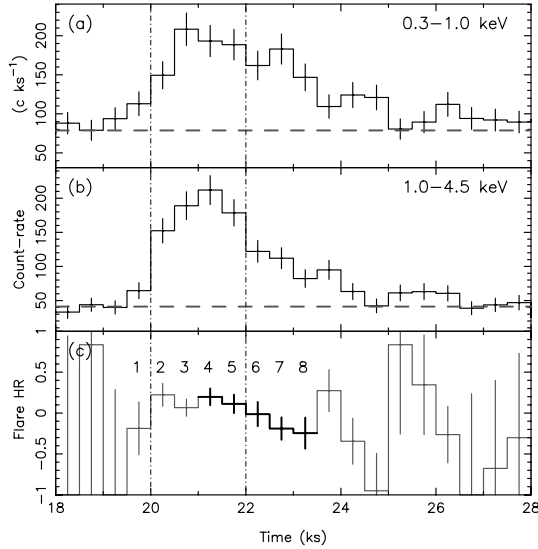
Figure 6. Time-series for the flare exhibited by H II 1032: (a) and (b) background-subtracted count-rates in the 0.3–1.0 and 1.0–4.5 keV bands, respectively; (c) hardness ratio, defined in the text. The mean quasi-steady value of count rate in each band is shown by dashed grey lines. The points used for analysis of the flare decay are shown in bold; numbers refer to points in Fig. 7. The interval used for the extraction of the flare-peak spectrum is bounded by dot–dashed lines.
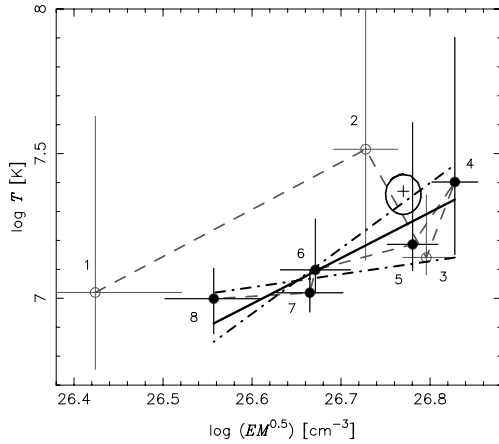

Figure 7. The evolution of estimated temperature (T) and electron density ($\propto \sqrt{EM}$) during the H II 1032 flare. T and EM were estimated from hardness ratio and count rate. Dashed grey lines connect sequential points; numbers refer to bins in Fig. 6. The slope, ζ, is a diagnostic for sustained heating through the flare decay. The points used to estimate ζ are shown in bold. The bold slope shows the best fit; the dot–dashed slopes are approximate 1σ limits. The ellipse shows the approximate 1σ confidence interval for parameters derived from the flare-peak spectrum.

the onset of the large flare that is discussed further in Section 4.2.2. H II 1032 exhibited a flare (Fig. 3b), with peak L_X a factor of ≈ 3 higher than the quasi-steady L_X, and $\tau_{LC} \approx 2$ ks, while the light curves of H II 1309 and 1514 displayed no *formal* variability (Figs 3d and e). The four flaring stars had higher quasi-steady $\log(L_X/L_{bol})$ values than the four non-flaring stars (see Table 3). The results follow the observed trend for more variability, and more frequent and larger flares in the coronae of more active stars (Stelzer et al. 2000).

4.2.1 Loop modelling from flare decays

The solar corona is highly structured with hot, X-ray-emitting plasma largely confined to magnetic loops that may span up to a third of the solar diameter (e.g. Reale et al. 1997). Although stellar coronae are not spatially resolved by present instrumentation, it has been shown that the sizes of magnetic loops involved in flares may be inferred from an analysis of the flare decay (van den Oord & Mewe 1989; Serio et al. 1991). Such techniques have typically neglected the presence of sustained heating in the decay and yielded loop half-lengths $\mathcal{L} > R_\star$ in stellar flares (e.g. GCS95). Reale et al. (1997) have performed detailed hydrodynamic modelling of the decay of flaring loops to develop an empirical method that diagnoses and accounts for continued heating in the estimation of loop sizes. The technique has been successfully tested on resolved solar flares and applied to stellar flares using a number of different X-ray detectors (including EPIC pn), yielding $\mathcal{L} < R_\star$ (e.g. Reale & Micela 1998; Favata & Schmitt 1999; Maggio et al. 2000; Güdel et al. 2001). The presence of sustained heating is diagnosed through the evolution of temperature, T, and density, n, in the flare decay, specifically the shallower the slope, ζ, in the $\log T$–$\log n$ diagram, the slower the decay time-scale of the flare heating rate (maximum $\zeta \approx 1.9$ for no continued heating; EPIC pn). For stellar flares n can rarely be directly measured so the emission measure, $EM = \int n_e n_H \, dV \propto n^2$, is used to obtain ζ from a $\log T$–$\log \sqrt{EM}$ diagram. $\mathcal{L}$ is then inferred from ζ, the light-curve decay time, τ_{LC}, and the maximum temperature in the loop at flare peak, T_{max}, as in equations (4) and (5) in Favata et al. (2000), where $c_A = 11.6$, $\zeta_A = 0.56$, $q_A = 1.2$ for EPIC pn (Reale, private communication).

The flares on H II 1032 and 1100 allow us to apply a modified version of the hydrodynamic technique to estimate the size of loop involved. For each flare, a spectrum of the flare 'peak' (displayed in grey in Figs 4b and f) was extracted and fitted with a single MEKAL component with Z fixed to the best-fitting quasi-steady value, in addition to the best-fitting quasi-steady model (from Table 3). The fitted temperatures (with 1σ confidence intervals) and emission measures of the plasma at flare peak were 23.5 (20–27) MK and 3.4×10^{53} cm^{-3} for H II 1032, and 15.4 (14–17) MK and 1.4×10^{53} cm^{-3} for H II 1100, from which we derived respective T_{max} values of 39.2 (32–46) and 24.3 (22–27) MK using the relation (Reale, private communication):

$$T_{max} = 0.184\, T_{obs}^{1.13}\,(\text{for EPIC pn}).$$

We constructed a $\log T$–$\log \sqrt{EM}$ diagram by estimating the flare temperature from a hardness ratio (HR $= (B - A)/(A + B)$, where A and B are the count-rates above the mean quasi-steady count rate in the 0.3–1.0 and 1.0–4.5 keV bands, respectively: Fig. 6), and then the emission measure for that temperature from the total count rate $A + B$. Conversions were calculated using the pn response appropriate for the particular star (Section 3.2) and 1-T MEKAL emission models with Z fixed to the best-fitting quasi-steady value. The count-rates were not sufficient to constrain ζ well: $\zeta_{1032} = 1.6$ (0.45–2.3) (Fig. 7); $\zeta_{1100} = 1.0$ (<1.6). Although in the H II 1032 flare ζ is consistent with the absence of sustained heating, its presence cannot be ruled out, and it is apparently required in the case of H II 1100. If $\zeta < 0.4$, the observed decay is controlled by the heating decay time-scale, not the thermodynamic time-scale, and is hence independent of $\mathcal{L}$, which can be constrained only by an upper limit: this is the case for H II 1100. To estimate the lower and upper bounds of a 1σ confidence interval for $\mathcal{L}$ we have first calculated the lower and upper bounds for the quantity $\mathcal{L}F(\zeta)$ using the 1σ uncertainties on T_{max} and τ_{LC}, secondly added in quadrature

a 20 per cent uncertainty that derives from consistency checks on solar flares, and finally used the lower and upper bounds of ζ to obtain upper and lower bounds, respectively, to $F(\zeta)$. We thus estimate $\mathcal{L}_{1032} \sim 1.8\ (0.4\text{–}2.6) \times 10^{10}$ cm $\sim 0.3\ (0.07\text{–}0.45)\ R_\star$ and $\mathcal{L}_{1100} \sim 1.2(<2.5) \times 10^{10}$ cm $\sim 0.25\,(<0.5)R_\star$. Assuming a loop aspect ratio of 0.2, the mean electron densities in the loop at flare peak, n, were $n_{1032} \sim 5\ (2.7\text{–}45)$ and $n_{1100} \sim 5\ (>2) \times 10^{11}$ cm^{-3}. The corresponding pressures, p, calculated from the equation of state, were $p_{1032} \sim 5\ (2.5\text{–}60)$ and $p_{1100} \sim 4\ (>1) \times 10^3$ dyne cm^{-2}, requiring magnetic field strengths, B, of $B_{1032} \sim 400\ (250\text{–}1200)$ and $B_{1100} \sim 300\ (>170)$ G for confinement. These values are fairly typical of a variety of larger flares on the nearby young K-type stars AB Dor ($\mathcal{L}$ in the range 2.5–4.9 $\times$ 10^{10} cm: Ortolani et al. 1998; Maggio et al. 2000; Güdel et al. 2001), and LQ Hya ($\mathcal{L} \approx 8.3 \times 10^{10}$ cm: Covino et al. 2001), which have been analysed using the hydrodynamic method.

We caution that *TRACE* images of large solar flares reveal structure far more complex than single loops (e.g. see the review by Aschwanden, Poland & Rabin 2001), and so stellar flares, often $10^{2\text{–}3}$ times more powerful than the strongest solar flares, may not be well-modelled as single loops.

4.2.2 An eclipse of the flare on H ɪɪ 1100?

The light curve of H ɪɪ 1100 displays a striking dip at 24–25.5 ks after the start of the pn exposure when the count rate drops sharply from ≈ 120 count ks^{-1} to the quasi-steady rate of ≈ 40 count ks^{-1} in $\tau_{\text{fall}} \approx 300$ s, remains at this value for $\tau_{\text{min}} \approx 600$ s, and then rises sharply to ≈ 200 count ks^{-1} in $\tau_{\text{rise}} \approx 500$ s (Fig. 3f). The feature is not of instrumental origin as it is reproduced in the MOS light curves, the background on that CCD shows no similar feature and no periods of data loss at this time were recorded.

The profile of the dip is suggestive of a total eclipse of a slow-rising flare, and the most interesting possibility is that this is caused by an object orbiting the flaring star. Approximating the flare geometry to the simplest case of a uniform circular source, and assuming a near-central eclipse, the ratio of radii of eclipsing object, R_b, and flare, R_{fl}, is

$$R_b/R_{\text{fl}} = 1 + \tau_{\text{min}}/\tau_{\text{fall}} \approx 3$$

while $R_b = (\tau_{\text{fall}} + \tau_{\text{min}})v/2$, where v is the orbital velocity of the eclipsing object. Substituting for v using Kepler's third law, the product of the circular orbital distance, a_b, and R_b^2 is

$$a_b R_b^2 = (\tau_{\text{fall}} + \tau_{\text{min}})^2 GM_\star(1 + M_b/M_\star)/4 \approx 22,$$

where a_b and R_b are measured in 10^{10} cm and $M_\star = 0.8\,\mathrm{M_\odot} \gg M_b$. The loop half-length, $\mathcal{L} = \pi R_{\text{fl}}/2 \sim 1.2 \times 10^{10}$ cm, inferred from the flare decay suggests $R_b \sim 2.3 \times 10^{10}$ cm and, unacceptably, $a_b \sim 4 \times 10^{10}$ cm, $< R_\star$, although the geometry of the loop and its inclination may cause $R_b/R_{\text{fl}} < 3$, and a smaller loop size was allowed by the flare-decay analysis. A Jupiter-sized object ($R_b = R_J \approx 0.7 \times 10^{10}$ cm) must orbit at a distance of $\sim$0.03 au to cause the eclipse, and would imply a flare-loop half-length of $\mathcal{L} \sim 0.4 \times 10^{10}$ cm, the flare decay hence being controlled by the heating decay time-scale, independent of the loop size. A number of such 'hot Jupiters' have been detected around nearby solar-like stars (e.g. 51 Peg b: Mayor & Queloz 1995; τ Boö b: Butler et al. 1997). Although H ɪɪ 1100 is a binary system, the projected separation of the near-twin components of 100 au (Bouvier et al. 1997) is too large to affect the orbit of such a planet. The existence of such a planet could be demonstrated by optical observations. Its transit across the stellar disc should eclipse a fraction $(0.7/5.0)^2 = 0.02$ of the disc area, causing a dimming

of 0.02 mag. Given the above orbit, this dimming should last $\sim$3 ks and occur every $\sim$2 d. The gravitational influence of the planet should also cause a small periodic radial velocity perturbation of $0.2M_b \sin i/M_J$ km s^{-1}, although the apparent magnitude of $V = 12.16$ for H ɪɪ 1100 makes such measurements extremely difficult. If a planet were to be confirmed, this would be the first planet detected by its eclipse of an X-ray flare, the first planet discovered in the Pleiades, and only the second planet discovered by a transit method. However, one must conclude that even if such a planet was to exist, its total eclipse of a flaring loop would be a highly fortuitous event.

An alternative possibility is that the flare was obscured by cool material passing across the line of sight, as proposed by Haisch et al. (1983) to explain the observation by *Einstein* of a temporarily increased N_H for a time interval during a flare on the dMe star Proxima Centauri. If we model the flare plasma using the best-fitting spectral model of the flare peak (Section 4.2.1), an absorbing column of $N_H > 10^{22}$ cm^2 is required to absorb >75 per cent of the 0.3–4.5 keV photons, as is observed. This is two orders of magnitude greater than has been seen in solar prominences, the Proxima Centauri event, or cool clouds in the atmosphere of AB Dor that have been inferred from transient Hα absorption profiles (Collier Cameron et al. 1990). While the size of the AB Dor clouds (area $\sim$10^{21} cm^2) is comparable to that required by our eclipse profile, their velocities, held to the rotation of the star at around the corotation radius, $\sim$200–300 km s^{-1}, are not analogous to the velocity of $\sim$150–500 km s^{-1} required of our obscuring cloud, as $v \sin i$ is only 5 km s^{-1} for H ɪɪ 1100. While such high velocities are fairly common in erupting prominences on the Sun (e.g. Gopalswamy et al. 2003), and the bulk kinetic energy of the cloud is around the same order of magnitude as (0.05–5 times) the total energy, $\sim$6 $\times$ 10^{33} erg, radiated by the flare with which it is presumably associated, it would be puzzling if such a flare, which is a routine twice-a-day occurrence on AB Dor, was associated with such an extraordinarily denser cloud.

A third explanation is that the large flare, with an impulsive, short rise-time, is shortly preceded by a smaller flare (albeit, with peak $L_X \approx 10^{30}$ erg s^{-1}, still larger than the flares exhibited by H ɪɪ 1516 and 1280) with a shorter decay time than rise time. Evidence for a further flare-like event occurring during the flare decay, at $\approx$27.8 ks (see Fig. 3f) supports the idea of multiple flaring within a complex active region. If we apply the hydrodynamic model with $T_{\text{max}} \sim 25$ MK, the fast decay, $\tau_{\text{fall}} \sim 300$ s, indicates a loop structure, $\mathcal{L} \lesssim 10^9$ cm $\lesssim 0.02R_\star$, smaller than that of the larger flare that followed, though similar to that inferred from a flare with peak $L_X \approx 4 \times 10^{29}$ erg s^{-1}, observed on a component of the dMe binary YY Gem (Stelzer et al. 2002). Flares with a longer rise than decay time do not form a well-recognized class on the Sun, but they have been occasionally observed on other stars (e.g. the dMe star EQ Peg: Pallavicini, Tagliaferri & Stella 1990; several examples in the Pleiades and Hyades noted by Stelzer et al. 2000). The coincidence of two flares – the first unusual, the second impulsive – in such a way as to mimic an eclipse forms a somewhat ad hoc explanation of the feature, but none of the available hypotheses presents a convincing explanation on the grounds of probability and/or precedent. A planetary eclipse is the most interesting possibility and the only one that may be confirmed or refuted by further observations.

4.3 Emission from intermediate-type stars?

Intermediate-type stars ($\approx$B4–F4) are believed to lack both the massive stellar wind and deep convective envelope intrinsic to the X-ray

Table 4. Physical and X-ray characteristics of intermediate-type Pleiads in the *Chandra* and *XMM–Newton* fields. Columns show: (2) spectral type of primary; (3) $v \sin i$ in km s^{-1}; (4) and (5) binarity flag and reference: 1. Abt et al. (1965); 2. Liu et al. (1991); 3. Mason et al. (1993); 4. Høg et al. (2000); 5. Dommanget & Nys (2000); (6) and (7) estimated primary and secondary masses (Raboud & Mermilliod 1998); (8) spectral type of secondary, inferred from M_2; (9) field; (10) and (11) best-fitting temperatures in keV for X-ray spectrum; (12) log L_X in the 0.5–2.0 keV band; (13) proposed spectral type of dominant X-ray source. *Chandra* data is from DLG02.

H II (1)	SpT$_A$ (2)	$v \sin i$ (3)	Bin. (4)	Ref. (5)	M_A (6)	M_B (7)	SpT$_B$ (8)	X-ray Obs (9)	kT_1 (10)	kT_2 (11)	log L_X (12)	SpT(X) (13)
1309	F6 V	85			1.21			*XMM–Newton*	<0.2	0.56	29.4	F
1122	F4 V	28	SB2	2	1.22	0.51	K/M	*Chandra*	–	0.45	29.1	F
1338	F3 V	10	SB2	2	1.22	1.22	F	*Chandra*	–	–	28.7	F
1762	A9 V	180	SB2, VB	2, 3	1.36	0.86	G/K	*XMM–Newton*	<0.2	0.64	29.6	G
1284	A9 V	100	SB1	2	1.45	0.86	G/K	*Chandra*	–	–	27.6	K
956	A7 V	150	SB?, VB	2, 4	1.37	1.18	F	*Chandra*	–	0.57	29.3	F
1362	A7 V	<12			1.52			*Chandra*	–	–	<27.9	
1384	A4 V	215			1.61			*XMM–Newton*	0.53	1.01	30.1	G
1028	A2 V	110	VB	3	1.86	1.45	A	*XMM–Newton*	–	–	<27.6	
1431	A0 V	40	SB2	1	1.97	0.68	K	*XMM–Newton*	–	–	<27.6	
1375	A0 V	160	SB1	2	2.11	1.74	A	*Chandra*	–	–	<28.0	
1234	B9.5 V	260	VB	3	2.11	1.33	A/F	*XMM–Newton*	0.37	1.08	29.4	K
980	B6 IV	275	VB	5	2.53	?	?	*Chandra*	–	0.56	29.6	G

generation mechanism of early-type and solar-like stars, respectively. Indeed, most X-ray surveys of A-type stars in the field and in open clusters have found a paucity of detections (e.g. Schmitt et al. 1985; Micela et al. 1990; Schmitt et al. 1990). The L_X of detected stars appears to be uncorrelated with stellar properties influential in the emission mechanisms of early-type or solar-like stars, such as L_{bol}, or rotation (Simon, Drake & Kim 1995; Panzera et al. 1999). However, chromospheric emission has been reported to show a correlation with rotation rate for stars with spectral types as early as A9 (Schrijver 1993), and emission lines of C III and O VI in τ^3 Eri indicate material at temperatures in excess of 0.3 MK is possible in the atmospheres of stars as early as A4 (Simon et al. 2002). In the Hyades, a sharp fall in chromospheric emission is observed to occur at spectral type F5, which coincides with a sharp fall in rotation velocity (Böhm-Vitense et al. 2002). It is possible that dynamo-driven coronal X-ray emission extends to spectral types with some subclasses earlier than F5. 95 per cent of all F-type stars within 13 pc of the Sun were detected by *ROSAT* (Schmitt 1997), although only an F2 subgiant and an unresolved pair of F0 V stars were earlier than F5. α Aqu (Altair) and α Cep were the only assuredly single A stars in the solar neighbourhood to be detected; both are fast-rotating, A7 stars with very cool, low-luminosity, coronae ($v \sin i > 210$ km s^{-1}, $kT \approx 0.1$ keV, $L_X \approx 2 \times 10^{27}$ erg s^{-1}: Simon et al. 1995). However, detected intermediate-type stars have usually had hotter temperatures and L_X of factors up to 10^{2-3} higher; similar to the most active solar-like stars. Hence, such detections have been conventionally attributed to coronal emission from late-type companions (e.g. Golub et al. 1983; Caillault & Zoonematkermani 1989; Caillault, Gagné & Stauffer 1994; Micela et al. 1996). In some cases further investigation has uncovered an active late-type companion (Güdel et al. 1998; Simon & Ayres 2000), but often no further evidence for an appropriate partner exists, and in *ROSAT* HRI studies of resolved late-B + late-type (*Lindroos*) binary systems, the B-type component was found to be the brighter X-ray source in many cases (Berghöfer & Schmitt 1994). However, one cannot rule out the existence of further late-type companions closer still to the primary, and hardness ratios of these X-ray-bright B-type stars are consistent with those of late-type coronae (Huélamo et al. 2000).

Three of the five intermediate-type stars in our observation were detected. We consider available optical and binarity information for these stars, in addition to our own X-ray spectral and timing data (Table 4), to test for consistency with a late-type companion. Where a companion is known, we have inferred an approximate spectral type from the estimated masses of Raboud & Mermilliod (1998).

4.3.1 H II 1762 (A9 V)

H II 1762 was close to the edge of the EPIC FOV and so only observed by MOS1. Its light curve showed no significant variability. Its X-ray spectrum was best-fitted by a 1-T $Z_\odot$ model with $kT \approx 0.64$ keV and log $L_X \approx 29.6$: both somewhat higher than found for H II 1514 and 1309. H II 1762 has a known spectroscopic and visually separated companion of estimated spectral type G–K: a G star more active than H II 1514 is a viable source of the X-ray emission.

4.3.2 H II 1384 (A4 V)

H II 1384 is one of the brightest X-ray sources in the Pleiades with log $L_X \approx 30.1$ reported in *Einstein*, *ROSAT* and *XMM–Newton* observations. A flare with peak log L_X of 30.5 and decay time of ≈ 1.2 ks was noted by Stelzer et al. (2000).

H II 1384 fell on the very edge of a pn CCD, which may have caused the variability not observed in the MOS light curves. Analyses of spectra from the pn, and from MOS1, and simultaneous fitting of the two MOS spectra were in good agreement, but the MOS2 spectrum required a hotter second component. A Z_{free} model was required to give an acceptable fit and the addition of a second component gave significant improvement. The spectral parametrization: $kT_1 \approx 0.5$, $kT_2 \approx 1.0$ keV, with $EM_2/EM_1 \sim 0.8$, and $Z \sim 0.25$ $Z_\odot$, is similar to that of coronae on fast-rotating G stars (Fig. 5), although no companion to H II 1384 has been found. Radial velocity variations of ~ 35 km s^{-1} reported by Abt et al. (1965) have been doubted (Simon et al. 1995; Raboud & Mermilliod 1998), and more recent studies, albeit based on just two measurements each, found no evidence for variations indicative of a close companion (Liu, Janes & Bania 1991; Morse, Mathieu & Levine 1991). Speckle interferometry revealed no companion at angular separations of 0.035–1 arcsec unless it is >3 mag fainter than the $V = 7.66$ primary (Mason et al. 1993), so a late-G star could have escaped detection. Fig. 2 does suggest photometric binarity. The apparently

extraordinary X-ray emission of H II 1384 could be explained by a highly active G-type companion, just like those discovered to accompany 47 Cas (Güdel et al. 1998) and the Hyad 71 Tau (Simon & Ayres 2000), two F0 stars with apparent L_X of 2×10^{30} erg s^{-1}. A dedicated radial velocity study of the star could test this hypothesis.

4.3.3 H II 1028 (A2 V)

H II 1028 showed no X-ray emission above a threshold log L_X of 27.6. A visual companion, estimated to be a late-A star, is also not expected to be a strong X-ray emitter.

4.3.4 H II 1431 (A0 V)

H II 1431 also showed no X-ray emission above a threshold log L_X of 27.6. This is somewhat surprising as it has a spectroscopic companion estimated to be a K star for which the X-ray emission would have to be among the faintest 5 per cent for K stars in the Pleiades according to the luminosity functions of Stauffer et al. (1994) and Stelzer & Neuhäuser (2001).

4.3.5 H II 1234 (B9.5 V)

H II 1234 showed a strong increase in X-ray output of a factor of ~ 2 toward the end of the observation (Fig. 3g). The quasi-steady spectrum required a second component or Z_{free} for an acceptable fit, and a significant improvement was found using a 2-T Z_{free} model. The log L_X of 29.5 and spectral parametrization: $kT_1 \approx 0.4$, $kT_2 \approx 1.1$ keV, with $EM_2/EM_1 \sim 1.5$ and $Z \sim 0.25$ $Z_{\odot}$, resemble those for an active K star (Fig. 5). Spectral parametrization of the higher emission state was poorly constrained but indicated higher temperatures (~ 0.7 and 2 keV), similar abundances and log $L_X \approx 29.7$. H II 1234 also has a visual companion of intermediate type and is not expected to be a strong X-ray source. The X-ray emission would be better explained by a hidden K-type companion in the system.

4.3.6 The combined Chandra and XMM–Newton sample

X-ray emission from the detected intermediate-type stars in the *XMM–Newton* observation appears to be consistent with coronal emission from companions of spectral types F, G or K. The inclusion of intermediate-type Pleiads in the *Chandra* field analysed by DLG02 more than doubles the sample size (Table 4). Our interpretation of the results from the combined sample is that the soft X-ray emission from the three F-type stars is probably dominated by coronal emission from the primaries (or the F-type companion in H II 1338), while the strong, soft X-ray emission of the A and B stars H II 956, 980 and 1762 is not intrinsic (as proposed by Krishnamurthi et al. 2001), but due to F-type, or moderately active G-type companions, which are probably identical with companions already noted in the literature. Conversely, the companions of H II 1431 and 1284 are unusually weak X-ray-emitters if they are truly K-type stars. The strong, harder emissions of H II 1234 and 1384 are plausibly due to highly active K- and G-type companions, respectively, but neither have yet been discovered. Dedicated radial velocity and interferometric studies are required to confirm the presence of such companions, in tandem with a wider *XMM–Newton* and/or *Chandra* X-ray spectroscopic survey of intermediate-type Pleiads to increase the sample size. If it can be firmly demonstrated that X-ray emission from intermediate-type stars is solely due to companions, X-ray studies may become an effective method of not only surveying the binarity status of stars in this mass range, but also constraining the spectral types of companions.

5 SUMMARY

We have performed detailed spectral and timing analyses of a sample of 13 intermediate-type and solar-like Pleiads, contained in a 40-ks *XMM–Newton* EPIC observation of the core of the cluster, that enabled the study of individual members with X-ray luminosities an order of magnitude lower than achieved using *ROSAT*. All solar-like members (one F, two G and five K stars) had $L_X \gtrsim 10^{29}$ erg s^{-1} and consistent with a rotation–activity connection: three ultrafast rotators emitted at a saturated level. Variable emission was observed from the K stars and fast-rotating G star, and the four with highest quasi-steady L_X/L_{bol} values exhibited flares. Hydrodynamic modelling of the flares on H II 1032 and 1100 led us to infer loop structures of half lengths $\mathcal{L} < 0.5 R_\star$. The light curve of H II 1100 showed a dip feature that could be due to an eclipse by a 'hot Jupiter'-like planet, absorption by a cool prominence with $N_H > 10^{22}$ cm^{-2} moving across the line of sight at several hundred km s^{-1}, or the coincidence of two flares, the first with an unusual decay, faster than its rise, indicating a small loop, $\mathcal{L} < 0.02 R_\star$. None of these explanations is satisfactory in likelihood or precedent, but the existence of a planet may be tested by optical photometric monitoring of the star for transits with a depth of ≈ 0.02 mag, followed by a spectroscopic search for radial velocity variations, though the star is faint ($V = 12.16$). Spectral modelling of the quasi-steady X-ray emission using two-temperature models: (i) confirmed the temperature sequence with spectral type (in order of rising temperature: F, slowly rotating G, K, fast-rotating G) deduced from composite spectra of Pleiades samples using the lower-resolution *ROSAT* PSPC and (ii) indicated subsolar metallicities. The results show that solar-like Pleiads conform to expectations from well-studied active solar-like stars, although none of the three UFRs had the hot, 2-keV component seen in the saturated coronae of the nearby stars AB Dor and 47 Cas. Three of the five intermediate-type Pleiads showed strong X-ray emission consistent with coronal emission from a solar-like companion. For such systems, the X-ray spectrum gives a useful insight into the spectral type of the companion.

REFERENCES

Abt H.A., Barnes R.C., Biggs E.S., Osmer P.S., 1965, ApJ, 142, 1604
Aschwanden M.J., Poland A.I., Rabin D.M., 2001, ARA&A, 39, 175

Audard M., Güdel M., 2002, in Jansen F., ed., New Visions of the X-ray Universe in the *XMM–Newton* and *Chandra* Era. ESA SP-488, in press

Belikov A.N., Hirte S., Meusinger H., Piskunov A.E., Schilbach E., 1998, A&A, 332, 575

Berghöfer T.W., Schmitt J.H.M.M., 1994, A&A, 292, L5

Böhm-Vitense E., Robinson R., Carpenter K., Mena-Werth J., 2002, ApJ, 569, 941

Briggs K.R., Pye J.P., 2003, ASR, in press

Bouvier J., Rigaut F., Nadeau D., 1997, A&A, 323, 139

Butler R.P., Marcy G.W., Williams E., Hauser H., Shirts P., 1997, ApJ, 474, L115

Caillault J.-P., Helfand D.J., 1985, ApJ, 289, 279

Caillault J.-P., Zoonematkermani S., 1989, ApJ, 338, L57

Caillault J.-P., Gagné M., Stauffer J.R., 1994, ApJ, 432, 386

Collier Cameron A., Duncan D.K., Ehrenfreund P., Foing B.H., Kuntz K.D., Penston M.V., Robinson R.D., Soderblom D.R., 1990, MNRAS, 247, 415

Covino S., Panzera M.R., Tagliaferri G., Pallavicini R., 2001, A&A, 371, 973

Cutri R.M. et al., 2000, Explanatory Supplement to the 2MASS Second Incremental Data Release. Caltech, Pasadena

Daniel K.J., Linsky J.L., Gagné M., 2002, ApJ, 578, 486 (DLG02)

Dommanget J., Nys O., 2000, A&A, 363, 991

Favata F., Schmitt J.H.M.M., 1999, A&A, 350, 900

Favata F., Reale F., Micela G., Sciortino S., Maggio A., Matsumoto H., 2000, A&A, 353, 987

Gagné M., Caillault J., Stauffer J.R., 1995, ApJ, 450, 217 (GCS95)

Gehrels N., 1986, ApJ, 303, 336

Girardi L., Bressan A., Bertelli G., Chiosi C., 2000, A&AS, 141, 371

Golub L., Harnden F.R., Maxson C.W., Vaiana G.S., Snow T.P., Rosner R., Cash W.C., 1983, ApJ, 271, 264

Gopalswamy N., Shimojo M., Lu W., Yashiro S., Shibasaki K., Howard R.A., 2003, ApJ, 586, 562

Güdel M., Guinan E.F., Skinner S.L., 1997, ApJ, 483, 947

Güdel M., Guinan E.F., Etzel P.B., Mewe R., Kaastra J.S., Skinner S.L., 1998, in Donahue R., Bookbinder J.A. eds, 10th Workshop on Cool Stars, Stellar Systems, and the Sun. Astron. Soc. Pac., San Francisco, p. 1247

Güdel M. et al., 2001, A&A, 365, L336

Haisch B.M., Linsky J.L., Bornmann P.L., Stencel R.E., Antiochos S.K., Golub L., Vaiana G.S., 1983, ApJ, 267, 280

Hertzsprung E., 1947, Ann. Sterrewacht Leiden, 19, 1

Høg E. et al., 2000, A&A, 355, L27

Huélamo N., Neuhäuser R., Stelzer B., Supper R., Zinnecker H., 2000, A&A, 359, 227

King J.R., Soderblom D.R., Fischer D., Jones B.F., 2000, ApJ, 533, 944

Kraft R.P., Burrows D.N., Nousek J.A., 1991, ApJ, 374, 344

Krishnamurthi A. et al., 1998, ApJ, 493, 914

Krishnamurthi A., Reynolds C.S., Linsky J.L., Martín E., Gagné, M., 2001, AJ, 121, 337

Liu T., Janes K.A., Bania T.M., 1991, ApJ, 377, 141

McKenzie D.L., Feldman U., 1992, ApJ, 389, 764

Maggio A., Pallavicini R., Reale F., Tagliaferri G., 2000, A&A, 356, 627

Marilli E., Catalano S., Frasca A., 1997, Mem. Soc. Astron. Ital., 68, 895

Mason B.D., Hartkopf W.I., McAlister H.A., Sowell J.R., 1993, AJ, 106, 637

Mayor M., Queloz D., 1995, Nat, 378, 355

Mewe R., Kaastra J.S., White S.M., Pallavicini R., 1996, 315, 170

Meyer J.-P., 1985, ApJS, 57, 173

Micela G., Sciortino S., Vaiana G.S., Harnden F.R., Rosner R., Schmitt J.H.M.M., 1990, ApJ, 348, 557

Micela G., Sciortino S., Kashyap V., Harnden F.R., Rosner R., 1996, ApJ, 102, 75

Micela G. et al., 1999, A&A, 341, 751

Monet D. et al., 1998, USNO-A V2.0, A Catalog of A. Donahue and J.A. Bookbinder Astrometric Standards, US Naval Observatory Flagstaff Station (USNOFS) and Universities Space Research Association (USRA) stationed at USNOFS

Morse J.A., Mathieu R.D., Levine S.E., 1991, 101, 1495

Noyes R.W., Weiss N.O., Vaughan A.H., 1984, ApJ, 287, 769

Orlando S., Peres G., Reale F., 2000, ApJ, 528, 524

Ortolani A., Pallavicini R., Maggio A., Reale F., White S.M., 1998, in Donahue A., Bookbinder J.A., eds, ASP Conf. Ser. Vol. 154, Cool Stars, Stellar Systems, and the Sun 10. Astron. Soc. Pac., San Francisco, p. 1532

Pallavicini R., Golub L., Rosner R., Vaiana G.S., Ayres T., Linsky J.L., 1981, ApJ, 248, 279

Pallavicini R., Tagliaferri G., Stella L., 1990, A&A, 228, 403

Panzera M.R., Tagliaferri G., Pasinetti L., Antonello E., 1999, A&A, 348, 161

Paresce F., 1984, AJ, 89, 1022

Parker E.N., 1975, ApJ, 198, 205

Pizzolato N., Maggio A., Micela G., Sciortino S., Ventura P., 2003, A&A, 397, 147

Queloz D., Allain S., Mermilliod J.-C., Bouvier J., Mayor M., 1998, A&A, 335, 183

Raboud D., Mermilliod J.-C., 1998, A&A, 329, 101

Reale F., 2002, in Favata F., Drake J., eds, ASP Conf. Ser. Vol. 277, Stellar Coronae in the, *Chandra* and *XMM–Newton* Era. Astron. Soc. Pac., San Francisco, p. 103

Reale F., Micela G., 1998, A&A, 334, 1028

Reale F., Betta R., Peres G., Serio S., McTiernan J., 1997, A&A, 325, 782

Reale F., Peres G., Orlando S., 2001, ApJ, 557, 906

Reames D.V., Meyer J.P., von Rosenvinge T.T., 1994, ApJS, 90, 649

Schmitt J.H.M.M., 1997, A&A, 318, 215

Schmitt J.H.M.M., Golub L., Harnden F.R., Jr, Maxson C.W., Rosner R., Vaiana G., 1985, ApJ, 290, 30

Schmitt J.H.M.M., Micela G., Sciortino S., Vaiana G.S., Harnden F.R., Rosner R., 1990, ApJ, 351, 492

Schrijver C.J., 1993, A&A, 269, 446

Serio S., Reale F., Jakimiec J., Sylwester B., Sylwester J., 1991, A&A, 241, 197

Simon T., Ayres T.R., 2000, ApJ, 539, 325

Simon T., Drake S.A., Kim P.D., 1995, PASP, 107, 1034

Simon T., Ayres T.R., Redfield S., Linsky J.L., 2002, ApJ, 579, 800

Singh K.P., Drake S.A., Gotthelf E.V., White N.E., 1999, ApJ, 512, 874

Soderblom D.R., Stauffer J.R., Hudon J.D., Jones B.F., 1993, ApJS, 85, 315

Stauffer J.R., 1984, ApJ, 280, 202

Stauffer J.R., Caillault J.-P., Gagné M., Prosser C.F., Hartmann L.W., 1994, ApJS, 91, 625

Stello D., Nissen P.E., 2001, A&A, 374, 105

Stelzer B., Neuhäuser R., 2001, A&A, 377, 538

Stelzer B., Neuhäuser R., Hambaryan V., 2000, A&A, 356, 949

Stelzer B. et al., 2002, A&A, 392, 585

Strüder L. et al., 2001, A&A, 365, L18

Terndrup D.M., Stauffer J.R., Pinsonneault M.H., Sills A., Yuan Y., Jones B.F., Fischer D., Krishnamurthi A., 2000, AJ, 119, 1303

Turner M.J.L. et al., 2001, A&A, 365, L27

van den Oord G.H.J., Mewe R., 1989, A&A, 213, 245

Vilhu O., 1984, A&A, 133, 117

This paper has been typeset from a TEX/LATEX file prepared by the author.